

Syntheses, Structure, Magnetism, and Optical Properties of the Ordered Interlanthanide Copper Chalcogenides $\text{Ln}_2\text{YbCuQ}_5$ ($\text{Ln} = \text{La, Ce, Pr, Nd, Sm}$; $\text{Q} = \text{S, Se}$): Evidence for Unusual Magnetic Ordering in $\text{Sm}_2\text{YbCuS}_5$

Geng Bang Jin,[†] Eun Sang Choi,[‡] Robert P. Guertin,[§] Corwin H. Booth,[⊥] and Thomas E. Albrecht-Schmitt^{*†}

[†]Department of Civil Engineering and Geological Sciences and Department of Chemistry and Biochemistry, University of Notre Dame, Notre Dame, Indiana, 46556, United States

[‡]Department of Physics and National High Magnetic Field Laboratory, Florida State University, Tallahassee, Florida 32310, United States

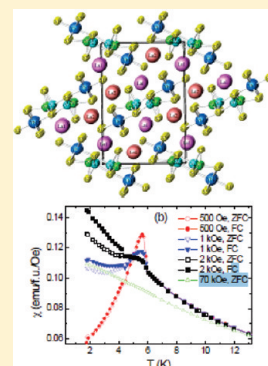
[§]Department of Physics and Astronomy, Tufts University, Medford, Massachusetts 02155, United States

[⊥]Chemical Sciences Division, Lawrence Berkeley National Laboratory, 1 Cyclotron Rd., Berkeley, California 94720, United States

S Supporting Information

ABSTRACT: $\text{Ln}_2\text{YbCuQ}_5$ ($\text{Ln} = \text{La, Ce, Pr, Nd, Sm}$; $\text{Q} = \text{S, Se}$) have been prepared by direct reaction of the elements in Sb_2Q_3 ($\text{Q} = \text{S, Se}$) fluxes at 900 °C. All compounds have been characterized by single-crystal X-ray diffraction methods and are isotypic. The structure of $\text{Ln}_2\text{YbCuQ}_5$ consists of one-dimensional $[\text{YbCuQ}_5]^{6-}$ ribbons extending along the b -axis that are connected by larger Ln^{3+} ions. Each ribbon is constructed from two single chains of $[\text{YbQ}_6]$ octahedra with one double chain of $[\text{CuQ}_5]$ trigonal bipyramids in the middle. All three chains connect with each other via edge-sharing. There are two crystallographically unique Ln atoms, one octahedral Yb site, and two disordered Cu positions inside of distorted Q_5 trigonal bipyramids. Both Ln atoms are surrounded by eight Q atoms in bicapped trigonal prisms. The magnetic properties of $\text{Ln}_2\text{YbCuQ}_5$ have been characterized using magnetic susceptibility and heat capacity measurements, while their optical properties have been explored using UV–vis–NIR diffuse reflectance spectroscopy. $\text{Ce}_2\text{YbCuSe}_5$, $\text{La}_2\text{YbCuS}_5$, $\text{Ce}_2\text{YbCuS}_5$, and $\text{Pr}_2\text{YbCuS}_5$ are Curie–Weiss paramagnets. $\text{La}_2\text{YbCuSe}_5$ and $\text{Nd}_2\text{YbCuS}_5$ show evidence for short-range antiferromagnetic ordering at low temperatures. $\text{Sm}_2\text{YbCuS}_5$ shows magnetic ordering at 5.9 K, followed by negative magnetization at low external fields. The band gaps of $\text{La}_2\text{YbCuSe}_5$, $\text{Ce}_2\text{YbCuSe}_5$, $\text{La}_2\text{YbCuS}_5$, $\text{Ce}_2\text{YbCuS}_5$, $\text{Pr}_2\text{YbCuS}_5$, $\text{Nd}_2\text{YbCuS}_5$, and $\text{Sm}_2\text{YbCuS}_5$ are 1.15, 1.05, 1.45, 1.37, 1.25, 1.35, and 1.28 eV, respectively.

KEYWORDS: structural characterization, magnetic materials, optical materials



INTRODUCTION

Rare-earth copper chalcogenides have been the source of considerable interest, not only because of their diverse structures and electronic properties, but also because of some unusual coordination geometries and oxidation states of copper that they exhibit.^{1–45} The large number of rare-earth copper chalcogenides can be divided into two groups, based on different interactions between chalcogenides. In the Group 1 phases, there are no Q–Q ($\text{Q} = \text{S, Se, Te}$) interactions. These compounds have been generally synthesized at relatively high temperatures as thermodynamically stable products, which include LnCuQ_2 ($\text{Ln} = \text{rare-earth}$; $\text{Q} = \text{S, Se, Te}$),^{1–16} $\text{Ln}_{0.66}\text{Cu}_2\text{S}_2$ ($\text{Ln} = \text{Gd, Er}$),^{17–20} and Eu_2CuQ_3 ($\text{Q} = \text{S, Se}$).^{21–23} LnCuQ_2 compounds adopt at least three different structures (monoclinic, orthorhombic, and trigonal), depending on the relative size of the Ln ions.^{1–16} Mixed-valency Eu_2CuQ_3 phases have Eu^{2+} and Eu^{3+} ions occupying two crystallographically independent sites, and Eu_2CuS_3 ²²

shows a ferromagnetic transition at 3.4 K, because of the coupling of Eu^{2+} ions. Group 2 compounds contain polychalcogenide anions with various degrees of Q–Q interactions, which are considered as kinetic products. These compounds have been typically prepared using alkali-metal/lanthanide halide fluxes or reactive fluxes, thereby allowing for lower reaction temperatures. Examples include La_2CuS_4 ,²⁵ Ln_3CuSe_6 ($\text{Ln} = \text{Sm, Gd, Tb, Dy}$),^{26–28} $\text{EuCu}_{0.66}\text{Te}_2$,²⁹ $\text{Gd}_3\text{Cu}_2\text{Te}_7$,³⁰ $\text{LaCu}_{0.28}\text{Te}_2$,³¹ and LnCu_xTe_2 ($\text{Ln} = \text{La, Nd, Sm, Gd, Tb, Dy}$).^{28,32} La_2CuS_4 features unusual discrete $[\text{S}_3\text{Cu}\cdots\text{S}-\text{S}\cdots\text{CuS}_3]^{12-}$ units, which contain two almost-planar $[\text{CuS}_3]^{5-}$ triangles bridged by a disulfide anion. $\text{EuCu}_{0.66}\text{Te}_2$ contains a flat square net of Te atoms, whereas all of the latter three have linear Te chains.

Received: November 22, 2010

Revised: January 7, 2011

Published: February 02, 2011

Partial substitutions of chalcogenides have been explored to access new phases with different physical properties from the parent ternary phase LnCuQ_2 (e.g., LaCuSTe and SmCuSTe).³³ Lanthanide copper oxychalcogenides including LnCuOQ ($\text{Ln} = \text{La, Ce, Pr, Nd}$; $\text{Q} = \text{S, Se, Te}$),^{34–44} $\text{La}_5\text{Cu}_6\text{O}_4\text{S}_7$,⁴⁵ and $\text{La}_3\text{CuO}_2\text{S}_3$ ⁴⁶ have been extensively studied. LnCuOQ compounds adopt a structure with alternately stacking PbO-like $[\text{Cu}_2\text{Q}_2]^{2-}$ layers and anti-PbO-like $[\text{Ln}_2\text{O}_2]^{2+}$ layers, which is similar to that of copper-based high- T_c superconducting oxides.^{34–44} LaCuOQ compounds are wide-band-gap p -type semiconductors, and they are considered to be potential transparent conductive materials.^{34–44} In contrast, $\text{La}_5\text{Cu}_6\text{O}_4\text{S}_7$ is metallic, and the average oxidation state of the Cu atoms is $+7/6$.⁴⁵

A different approach to prepare new quaternary rare-earth copper chalcogenides is to partially replace the heavy metal in known ternary phases with different rare-earth elements. To our knowledge, EuLnCuS_3 ($\text{Ln} = \text{Y, Gd–Lu}$)²⁴ are the only known examples of interlanthanide copper chalcogenides, which were made by replacing the Eu^{3+} ions in Eu_2CuS_3 , using other trivalent Ln atoms. The purpose of this study is to prepare new ordered quaternary interlanthanide copper chalcogenide phases by including two Ln atoms from opposite ends of the lanthanide series, which tend to have different coordination geometries in same compounds. Here, we present the syntheses, structure, optical, magnetic, and heat capacity measurements of the new quaternary interlanthanide copper chalcogenides, $\text{Ln}_2\text{YbCuQ}_5$ ($\text{Ln} = \text{La, Ce, Pr, Nd, Sm}$; $\text{Q} = \text{S, Se}$)

EXPERIMENTAL SECTION

Starting Materials. La (99.9%, Alfa-Aesar), Ce (99.9%, Alfa-Aesar), Pr (99.9%, Alfa-Aesar), Nd (99.9%, Alfa-Aesar), Sm (99.9%, Alfa-Aesar), Yb (99.9%, Alfa-Aesar), Cu (99%, Alfa-Aesar), S (99.5%, Alfa-Aesar), Se (99.5%, Alfa-Aesar), and Sb (99.5%, Alfa-Aesar) were used as received. The Sb_2Q_3 ($\text{Q} = \text{S, Se}$) fluxes were prepared from the direct reaction of the elements in sealed fused-silica ampules at 850 °C.

Syntheses. $\text{Ln}_2\text{YbCuQ}_5$ ($\text{Ln} = \text{La, Ce, Pr, Nd, Sm}$; $\text{Q} = \text{S, Se}$) were prepared using Sb_2Q_3 ($\text{Q} = \text{S, Se}$) fluxes. A total of 150 mg of Ln, Yb, Cu, and Q was stoichiometrically mixed with 75 mg of Sb_2Q_3 in fused-silica ampules in an argon-filled glovebox. The ampules were sealed under vacuum and placed in a programmable tube furnace. The following

heating profile was used: 2 °C/min to 500 °C (held for 1 h), 0.5 °C/min to 900 °C (held for 7 d), 0.04 °C/min to 500 °C (held for 2 d), and 0.5 °C/min to 24 °C. In each reaction, the major phases included high yields of black crystals of desired products and unreacted Sb_2Q_3 lying in the bottom of the ampules. This separation was achieved by slightly tilting the furnaces. Powder X-ray diffraction (XRD) measurements were used to confirm phase purity by comparing the powder patterns calculated from the single-crystal X-ray structures with the experimental data. Semiquantitative scanning electron microscopy coupled with energy-dispersive X-ray spectroscopy (SEM/EDX) analyses were performed using JEOL Model 840/Link Isis or JEOL Model JSM-7000F instruments. Ln, Yb, Cu, and Q percentages were calibrated against standards. Sb was not detected in the crystals. The Ln:Yb:Cu:Q ratios were determined to be approximately 2:1:1:5 from EDX analyses.

Crystallographic Studies. Single crystals of $\text{Ln}_2\text{YbCuQ}_5$ ($\text{Ln} = \text{La, Ce, Pr, Nd, Sm}$; $\text{Q} = \text{S, Se}$) were mounted on glass fibers with epoxy and optically aligned on a Bruker Model APEX single-crystal X-ray diffractometer, using a digital camera. Initial intensity measurements were performed using graphite-monochromated Mo $K\alpha$ ($\lambda = 0.71073$ Å) radiation from a sealed tube and monocrapillary collimator. SMART (v 5.624) was used for preliminary determination of the cell constants and data collection control. The intensities of reflections of a sphere were collected by a combination of three sets of exposures (frames). Each set had a different ϕ angle for the crystal and each exposure covered a ω range of 0.3°. A total of 1800 frames were collected, with exposure times of 10 or 20 s per frame, depending on the crystal.

For $\text{Ln}_2\text{YbCuQ}_5$, determination of integrated intensities and global refinement were performed with the Bruker SAINT (v 6.02) software package, using a narrow-frame integration algorithm. These data were treated first with a face-indexed numerical absorption correction using XPREP,⁴⁷ followed by a semiempirical absorption correction using SADABS.⁴⁸ The program suite SHELXTL (v 6.12) was used for space group determination (XPREP), direct methods structure solution (XS), and least-squares refinement (XL).⁴⁷ The final refinements included anisotropic displacement parameters for all atoms and secondary extinction. Some crystallographic details are given in Table 1. As an example, atomic coordinates and equivalent isotropic displacement parameters for $\text{La}_2\text{YbCuS}_5$ are given in Table 2. Additional crystallographic details can be found in the Supporting Information.

Powder X-ray Diffraction. Powder X-ray diffraction (XRD) patterns were collected with a Rigaku Model Miniflex powder X-ray diffractometer, using Cu $K\alpha$ ($\lambda = 1.54056$ Å) radiation.

Table 1. Crystallographic Data for $\text{Ln}_2\text{YbCuQ}_5$ ($\text{Ln} = \text{La, Ce, Pr, Nd, Sm}$; $\text{Q} = \text{S, Se}$)

formula	$\text{La}_2\text{YbCuSe}_5$	$\text{Ce}_2\text{YbCuSe}_5$	$\text{La}_2\text{YbCuS}_5$	$\text{Ce}_2\text{YbCuS}_5$	$\text{Pr}_2\text{YbCuS}_5$	$\text{Nd}_2\text{YbCuS}_5$	$\text{Sm}_2\text{YbCuS}_5$
fw	909.20	911.62	674.70	677.12	678.70	685.36	697.58
color	black	black	black	black	black	black	black
crystal system	orthorhombic	orthorhombic	orthorhombic	orthorhombic	orthorhombic	orthorhombic	orthorhombic
space group	$Pnma$ (No. 62)	$Pnma$ (No. 62)	$Pnma$ (No. 62)	$Pnma$ (No. 62)	$Pnma$ (No. 62)	$Pnma$ (No. 62)	$Pnma$ (No. 62)
a (Å)	12.1326(11)	12.1113(7)	11.615(4)	11.5616(13)	11.547(2)	11.5466(8)	11.5323(8)
b (Å)	4.1119(4)	4.0780(3)	3.9662(13)	3.9304(4)	3.9071(8)	3.8927(3)	3.8531(3)
c (Å)	17.6653(16)	17.5714(11)	16.923(6)	16.8423(18)	16.795(3)	16.7597(11)	16.6470(12)
V (Å ³)	881.29(14)	867.85(10)	779.6(5)	765.34(14)	757.7(3)	753.31(9)	739.71(9)
Z	4	4	4	4	4	4	4
T (K)	193	193	193	193	193	193	193
λ (Å)	0.71073	0.71073	0.71073	0.71073	0.71073	0.71073	0.71073
ρ_{calcd} (g cm ⁻³)	6.853	6.977	5.748	5.877	5.950	6.043	6.264
μ (cm ⁻¹)	429.51	442.61	265.47	277.73	288.98	299.16	323.04
$R(F)^a$	0.0369	0.0290	0.0261	0.0242	0.0317	0.0250	0.0263
$R_w(F_o^2)^b$	0.0966	0.0757	0.0628	0.0588	0.0736	0.0566	0.0665

$$^a R(F) = \sum ||F_o| - |F_c|| / \sum |F_o| \text{ for } F_o^2 > 2\sigma(F_o^2). \quad ^b R_w(F_o^2) = [\sum [w(F_o^2 - F_c^2)^2] / \sum wF_o^4]^{1/2}.$$

Magnetic Susceptibility Measurements. Magnetic data were measured on $\text{Ln}_2\text{YbCuQ}_5$ ($\text{Ln} = \text{La, Ce, Pr, Nd, Sm; Q} = \text{S, Se}$) powders in gelcap sample holders with a Quantum Design MPMS magnetometer/susceptometer between 2 K and 300 K and in applied fields up to 7 T. DC susceptibility measurements were made under zero-field-cooled (ZFC) conditions with an applied field of 0.1 T. Susceptibility values were corrected for the sample diamagnetic contribution, according to Pascal's constants,⁴⁹ as well as for the sample holder diamagnetism. Weiss temperature (θ_w) values were obtained from extrapolations from fits between 100 K and 300 K.

The heat capacity measurement was done for $\text{Sm}_2\text{YbCuS}_5$, using a Quantum Design PPMS. The powder sample was mixed with N grease as binding material, whose contribution to the total heat capacity was measured before the sample was mounted.

UV–vis–NIR Diffuse Reflectance Spectroscopy. The diffuse reflectance spectra for $\text{Ln}_2\text{YbCuQ}_5$ ($\text{Ln} = \text{La, Ce, Pr, Nd, Sm; Q} = \text{S, Se}$) were measured from 200 nm to 2500 nm, using a Shimadzu Model UV3100 spectrophotometer equipped with an integrating sphere attachment. The Kubelka–Munk function was used to convert diffuse reflectance data to absorption spectra.⁵⁰

RESULTS AND DISCUSSION

Structures of $\text{Ln}_2\text{YbCuQ}_5$ ($\text{Ln} = \text{La, Ce, Pr, Nd, Sm; Q} = \text{S, Se}$). The compounds $\text{Ln}_2\text{YbCuQ}_5$ ($\text{Ln} = \text{La, Ce, Pr, Nd, Sm}$;

$\text{Q} = \text{S, Se}$) are isotypic and crystallize in the centrosymmetric, orthorhombic space group $Pnma$. As illustrated in Figure 1, the structure can be described as being composed of one-dimensional (1D) $[\text{YbCuQ}_5]^{6-}$ ribbons running down the $[010]$ direction that are separated by Ln^{3+} ions. It includes two crystallographically unique Ln atoms, one octahedral Yb site, and two Cu positions. The polyhedra of Ln and Cu atoms are shown in Figure 2. Both Ln^{3+} cations are eight-coordinated and occur as bicapped trigonal prisms. The bond distances of LnQ_8 and YbQ_6 for $\text{Ln}_2\text{YbCuQ}_5$ are normal (see Table S1 in the Supporting Information). For example, in the case of $\text{La}_2\text{YbCuS}_5$, La–S distances range from 2.9046(16) Å to 3.241(2) Å, and Yb–S distances are in the range of 2.6311(16) Å to 2.7989(17) Å. These bond lengths are comparable to the sum of the ionic radii,⁵¹ 3.00 Å for LaS_8 and 2.70 Å for YbS_6 . Two Cu atoms are very close to each other, with the Cu(1)–Cu(2) distance being 0.841(3) Å in the case of $\text{La}_2\text{YbCuS}_5$. Obviously, these two sites cannot be occupied simultaneously. The occupancy of Cu(1) ranges from 0.19 to 0.54. Each Cu has a highly distorted tetrahedral environment. For example, the four Cu(1)–S distances for $\text{La}_2\text{YbCuS}_5$ are 2.257(3), 2.3464(18), 2.3464(18), and 2.544(4) Å, and S–Cu(1)–S angles are in the range of 90.78–(11)°–116.16(8)°. These bond distances are closer to the average values for Cu with triangular coordination (e.g., 2.33 Å in $\text{Cu}_2\text{S}^{52,53}$) than those for Cu with tetrahedral coordination (2.44 Å, according to Shannon⁵¹). Since there are no Q–Q bonds or Cu–Cu interactions, the oxidation states for each atom in $\text{Ln}_2\text{YbCuQ}_5$ can be assigned as +3/+3/+1/–2, respectively.

Similar coordination environments for Cu atoms in the structure of $\text{Ln}_2\text{YbCuQ}_5$ have been found in other lanthanide copper chalcogenides. Examples include Ln_3CuSe_6 ($\text{Ln} = \text{Sm, Gd, Tb, Dy}$),^{26–28} $\text{Gd}_3\text{Cu}_2\text{Te}_7$,³⁰ $\text{LaCu}_{0.28}\text{Te}_2$,³¹ and LnCu_xTe_2 ($\text{Ln} = \text{La, Nd, Sm, Gd, Tb, Dy}$),^{28,32} in which two disordered Cu sites are equivalent and the tetrahedra are less distorted. To better describe the connectivity among the polyhedra, Cu(1) and Cu(2) atoms can be considered as one average Cu site sitting in the cavities of a distorted trigonal bipyramid, as shown in Figure 2. The one-dimensional $[\text{YbCuQ}_5]^{6-}$ ribbons, which are shown in Figure 3a, consist of two single $[\text{YbQ}_6]$ octahedral chains with one double $[\text{CuQ}_5]$ trigonal bipyramidal chain in the middle. All three chains are connected to each other via edge-sharing. Within the $[\text{YbQ}_6]$ octahedral chain, each unit shares edges with two

Table 2. Atomic Coordinates and Equivalent Isotropic Displacement Parameters for $\text{La}_2\text{YbCuS}_5$

atom (site)	x	y	z	U_{eq} (Å ²) ^a	occupancy
La(1)	0.97977(4)	–0.25	0.82545(3)	0.00691(14)	1
La(2)	0.86754(4)	0.25	0.40038(3)	0.00686(14)	1
Yb(1)	0.80240(3)	0.25	0.63683(2)	0.01060(13)	1
Cu(1)	0.6657(2)	–0.25	0.51632(13)	0.0144(4)	0.54
Cu(2)	0.5960(3)	–0.25	0.50288(17)	0.0177(6)	0.46
S(1)	1.01210(17)	0.25	0.69895(13)	0.0066(4)	1
S(2)	0.81356(17)	–0.75	0.88370(13)	0.0072(4)	1
S(3)	0.88403(18)	–0.25	0.53444(13)	0.0104(4)	1
S(4)	0.59555(18)	0.25	0.57265(13)	0.0084(4)	1
S(5)	0.73861(18)	–0.25	0.72916(13)	0.0076(4)	1

^a U_{eq} is defined as one-third of the trace of the orthogonalized U_{ij} tensor.

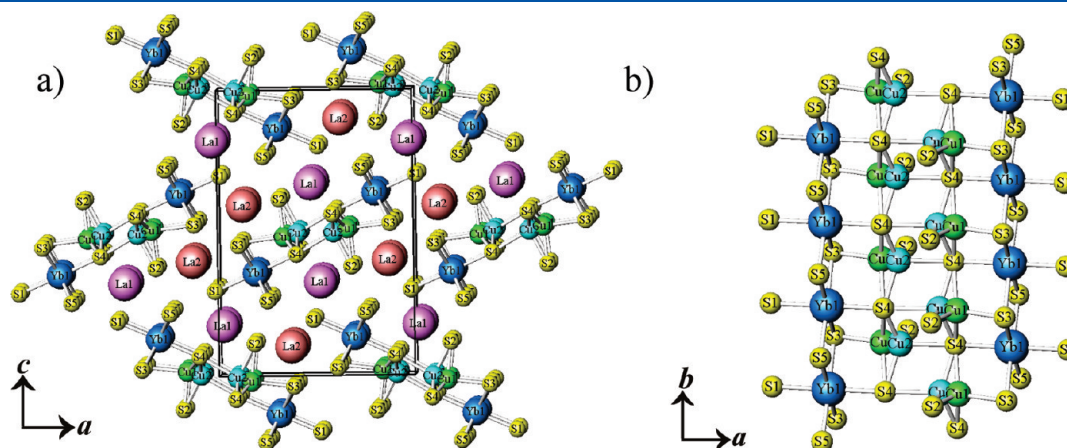


Figure 1. (a) View of the three-dimensional structure of $\text{La}_2\text{YbCuS}_5$ along the b -axis. It consists of one-dimensional $[\text{YbCuS}_5]^{6-}$ ribbons running down the $[010]$ direction that are separated by La^{3+} ions. La–S bonds have been omitted for clarity. (b) Depiction of an individual $[\text{YbCuS}_5]^{6-}$ ribbon.

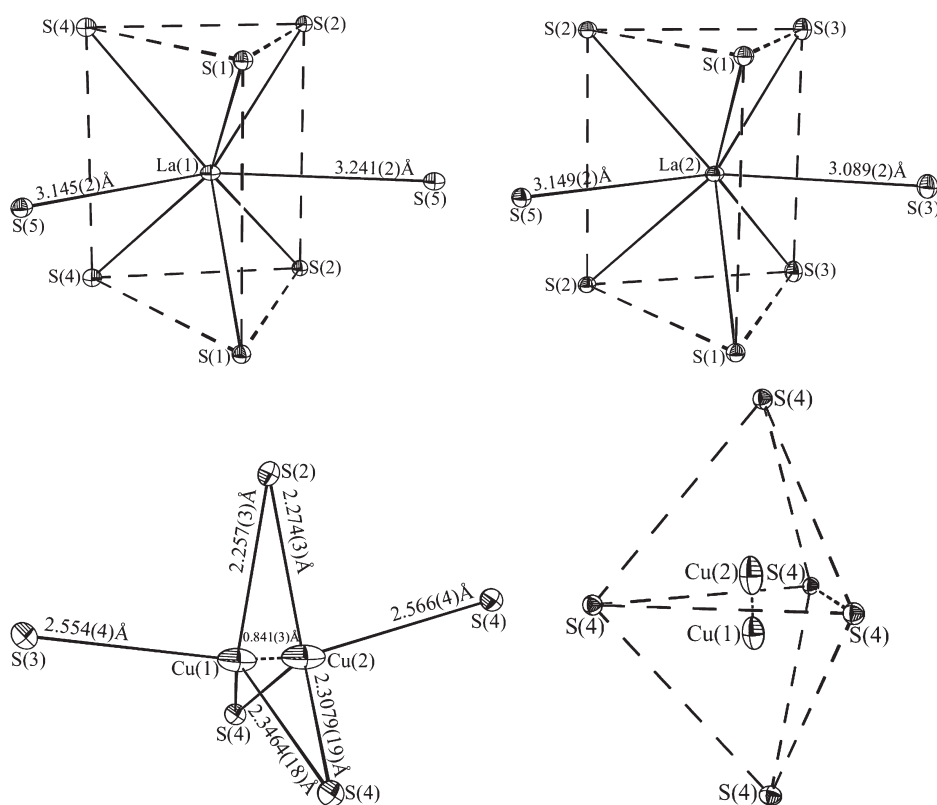


Figure 2. Illustrations of the coordination environments for La and Cu ions in $\text{La}_2\text{YbCuS}_5$.

neighbors along the chain direction, while each $[\text{CuQ}_5]$ trigonal bipyramid shares corners along the b -axis and shares edges with adjacent identical chains. The connectivity of $[\text{CuQ}_5]$ trigonal bipyramids in these compounds is quite different from other known examples. For $\text{Gd}_3\text{Cu}_2\text{Te}_7$,³⁰ the $[\text{CuTe}_5]$ trigonal bipyramids share corners with four $[\text{CuTe}_4]$ tetrahedra within two-dimensional $[\text{Cu}_2\text{Te}_5]$ layers (see Figure 3b). In Figure 3c, $[\text{CuSe}_5]$ trigonal bipyramids in Sm_3CuSe_6 ²⁶ share edges to form 1D single chains along the $[010]$ direction, while Figure 3d shows a two-dimensional (2D) $[\text{Cu}_x\text{Te}_2]$ layer in $\text{LaCu}_{0.28}\text{Te}_2$ ³¹ or LnCu_xTe_2 ($\text{Ln} = \text{La}, \text{Nd}, \text{Sm}, \text{Gd}, \text{Tb}, \text{Dy}$),^{28,32} constructed from $[\text{CuTe}_5]$ trigonal bipyramids sharing edges with four close neighbors and sharing corners with other four bipyramidal units.

$\text{Ln}_2\text{YbCuQ}_5$ are isotopic with the recently reported indium compounds, $\text{Ln}_2\text{InCuQ}_5$ ($\text{Ln} = \text{La}, \text{Ce}, \text{Pr}, \text{Nd}, \text{Sm}; \text{Q} = \text{S}, \text{Se}$),^{54–56} which is not surprising, considering the similar sizes of Yb^{3+} (1.01 Å) and In^{3+} (0.94 Å).⁵¹ In the structure of $\text{Ln}_2\text{InCuS}_5$, Cu atoms disorder into two close positions as the title ytterbium phases.⁵⁴ In contrast, the Cu position in $\text{La}_2\text{InCuSe}_5$ is fully occupied and ordered.⁵⁶

Note that $\text{La}_3\text{CuO}_2\text{S}_3$ ⁴⁶ adopts a similar formula and the same space group as $\text{Ln}_2\text{YbCuQ}_5$; however, their structures are clearly different. In the structure of $\text{La}_3\text{CuO}_2\text{S}_3$, there are three eight-coordinate La^{3+} ions with bicapped trigonal prismatic geometry, as illustrated in Figure 4. In contrast, the Yb ion in $\text{Ln}_2\text{YbCuQ}_5$ is only six-coordinated, because of its smaller size. Furthermore, the structure of $\text{La}_3\text{CuO}_2\text{S}_3$ only has one four-coordinated Cu^+ site in a regular $[\text{CuS}_4]$ tetrahedron, while there are two disordered Cu positions with highly distorted tetrahedral coordination in the structure of $\text{Ln}_2\text{YbCuQ}_5$. The structure of $\text{La}_3\text{CuO}_2\text{S}_3$ can be considered as a three-dimensional (3D) framework of face- and edge-sharing $\text{LaO}_n\text{S}_{8-n}$ polyhedra, within which the interstitial

space is filled by isolated one-dimensional chains of corner-sharing $[\text{CuS}_4]$ tetrahedra along the $[010]$ direction.

Magnetic Susceptibility. The inverse molar Ln magnetic susceptibilities for $\text{Ln}_2\text{YbCuQ}_5$ ($\text{Ln} = \text{La}, \text{Ce}, \text{Pr}, \text{Nd}; \text{Q} = \text{S}, \text{Se}$) in the range of 2–300 K are shown in Figures 5–7. The inverse molar Ln magnetic susceptibilities for $\text{Ln}_2\text{YbCuQ}_5$ ($\text{Ln} = \text{La}, \text{Ce}, \text{Pr}, \text{Nd}; \text{Q} = \text{S}, \text{Se}$) in the range of 2–300 K are shown in Figures 5–7. All six compounds show similar overall temperature dependence: Curie–Weiss-type susceptibility (linear behavior of inverse susceptibility) above 100 K, with deviation from the linear behavior below ~ 70 K. There is no evidence of magnetic ordering for $\text{Ce}_2\text{YbCuSe}_5$, $\text{La}_2\text{YbCuS}_5$, $\text{Ce}_2\text{YbCuS}_5$, and $\text{Pr}_2\text{YbCuS}_5$. In contrast, the magnetic susceptibilities for $\text{La}_2\text{YbCuSe}_5$ and $\text{Nd}_2\text{YbCuS}_5$ show changes in the slope at low temperature, which may indicate short-range antiferromagnetic ordering. The deviation of the Curie–Weiss law is most likely from a crystal electric field (CEF) effect of Ln^{3+} and/or Yb^{3+} ions. The CEF effect is presumably stronger for the Yb^{3+} ion (which is located in the center of YbQ_6 octahedron) than that of a Ln^{3+} ion under a more-complicated (lower-symmetry) crystal field of Q^{2-} .

Under the cubic crystal field environment, the $^2\text{F}_{7/2}$ multiplet of the Yb^{3+} ion will split into two doublets and one quartet with a Kramers doublet ground state.⁵⁷ As a result, the spins are populated over the different CEF levels, giving smaller effective moments when the thermal energy is smaller than the CEF splitting. One can fit the temperature dependence of magnetic susceptibility with a full knowledge of CEF scheme, using the van Vleck formalism. Instead, we can exploit the linear behavior between 100 K and 300 K to estimate magnetic parameters (effective moment (P_{eff}) and Weiss temperature (θ_p)), using the Curie–Weiss law, whose results are tabulated in Table 3, along

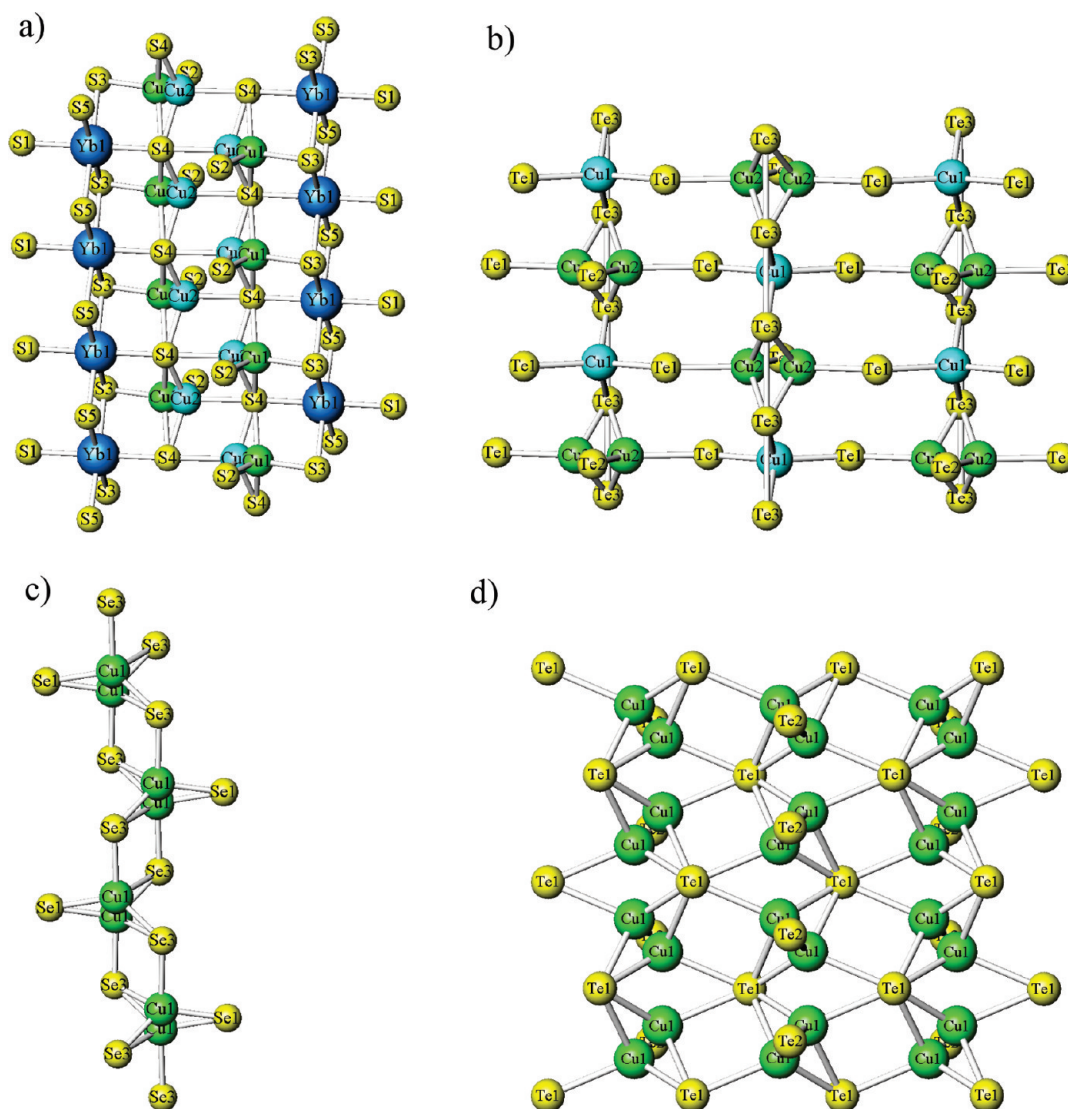


Figure 3. Depictions of various connectivities of $[\text{CuQ}_5]$ ($\text{Q} = \text{S}, \text{Se}, \text{Te}$) trigonal bipyramids in different compounds: (a) $\text{La}_2\text{YbCuS}_5$, (b) $\text{Gd}_3\text{Cu}_2\text{Te}_7$,³⁰ (c) Sm_3CuSe_6 ,²⁶ and (d) $\text{LaCu}_{0.28}\text{Te}_2$.³¹

with the calculated effective moment from free Ln^{3+} and Yb^{3+} ions. The good agreement of the effective moment values between the experimental results and calculation indicates that the highest excited CEF level is well below 100 K and the spins are well-populated over the CEF levels at >100 K.

On the other hand, at low temperatures, the spin is populated only at low-lying CEF levels, resulting in a reduced effective moment. There is a linear inverse susceptibility behavior at narrow temperature ranges between 5 and 20 K, where we derived the magnetic parameters and tabulated them in Table 3. Both the effective moment and the Weiss temperature are reduced, as expected. For nonmagnetic La^{3+} compounds ($\text{La}_2\text{YbCuQ}_5$), the effective moment is reduced further for the $\text{Q} = \text{S}$ compound, which is expected, because of a shorter distance between Yb^{3+} and S^{2-} . It is difficult to perform further analyses because the CEF effects of both Ln^{3+} and Yb^{3+} are involved at low temperatures.

The low-temperature magnetic properties of $\text{Sm}_2\text{YbCuS}_5$ show very different behavior from the other compounds. As shown in Figure 8, the high-temperature inverse susceptibility looks

similar to other compounds, except for a more rapid decrease below 7 K. Subsequent detailed measurements at ~ 7 K revealed anomalous behaviors, especially at low fields. The results at representative fields are shown in Figure 9. The notable features are as follows: (1) abrupt increase of susceptibility below 5.9 K; (2) upon further cooling, the susceptibility shows a field-dependent peak (5.7 K at 50 Oe, 5.3 K at 2 kOe), followed by negative susceptibility (magnetization reversal) at 50 and 100 Oe fields; and (3) for 1 and 2 kOe, the susceptibility increases again with decreased temperatures. As the field increases, the anomalies become less significant and the susceptibility peak just below 5.9 K becomes a small bump at 70 kOe.

To identify the thermodynamic nature of these anomalies, we carried out heat-capacity measurements and the results are shown in Figure 10. The λ -shaped jump in the heat capacity suggests long-range magnetic ordering in this material. The magnetic entropy change (ΔS) was determined through the relation

$$\Delta S = \int \frac{C_p - C_{ph}}{T} dT$$

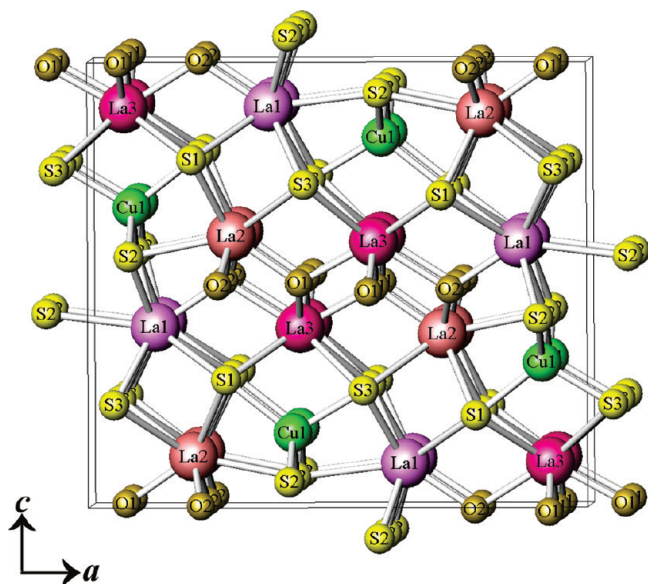


Figure 4. Unit cell of $\text{La}_3\text{CuO}_2\text{S}_3$ ⁴⁶ viewed along the *b*-axis.

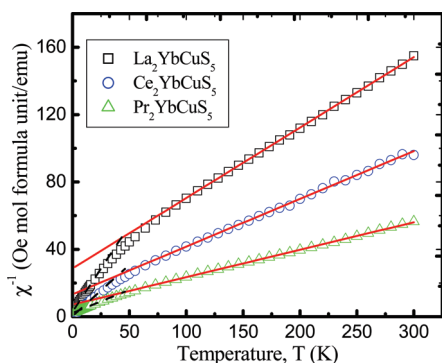


Figure 5. Inverse molar magnetic susceptibility versus temperature between 2 K and 300 K for $\text{La}_2\text{YbCuS}_5$, $\text{Ce}_2\text{YbCuS}_5$, and $\text{Pr}_2\text{YbCuS}_5$. Data were taken under an applied magnetic field of 0.1 T. The straight and dashed lines represent the fits to the Curie–Weiss law in the range of 100–300 K and 5–12 K, respectively.

where C_{ph} is the lattice contribution to the heat capacity. Using an empirical curve for the lattice contribution shown in Figure 10, we obtained $\Delta S = 1.13 R$ ($R = 8.31 \text{ J}/(\text{K mol})$). In the case of long-range ordering of magnetic ions with a total angular momentum J , ΔS is expressed as $\Delta S = R \ln(2J + 1)$. The J values for the free ions give larger values of ΔS ($J = 5/2$, $\Delta S = 3.6 R$ for Sm^{3+} , $J = 7/2$, $\Delta S = 2.1 R$ for Yb^{3+}). The observed smaller ΔS is presumably due to a CEF effect, which is consistent with the reduced effective moments at low temperatures.

The abrupt increase of susceptibility data and the λ -shape of the jump in the heat capacity at 5.9 K suggest a transition to long-range magnetic order with finite magnetic moments aligned to the external field with $T_c = 5.9 \text{ K}$. This type of behavior was reported in some systems with two magnetic sublattices, including perovskite manganites (SmMnO_3),⁵⁸ Prussian Blue analogues,^{59,60} ThCr_2Si_2 -type phosphides,⁶¹ and so forth. In SmMnO_3 , an antiferromagnetic coupling between weak ferromagnetic Mn ions and paramagnetic Sm ions was suggested to explain the temperature-induced magnetization reversal. Although we do not

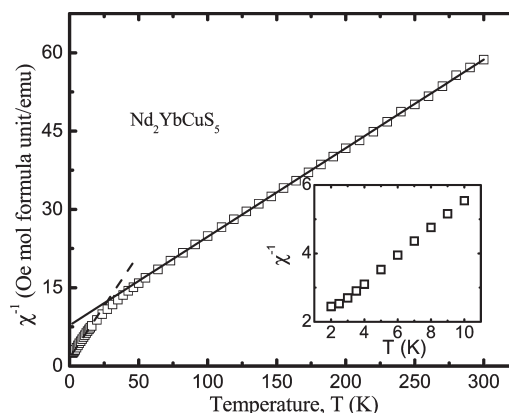


Figure 6. Inverse molar magnetic susceptibility versus temperature, showing the fit for $\text{Nd}_2\text{YbCuS}_5$, as in Figure 5. Inset shows the inverse molar magnetic susceptibility at low temperature.

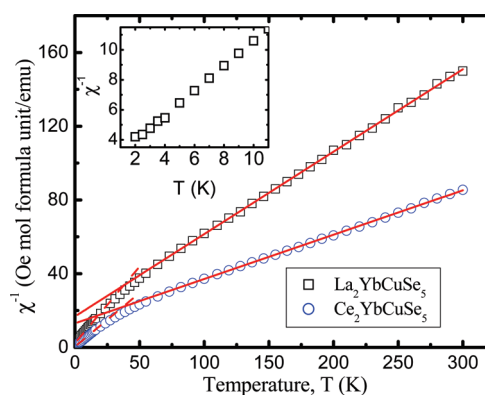


Figure 7. Inverse molar magnetic susceptibility versus temperature, showing the fit for $\text{La}_2\text{YbCuSe}_5$ and $\text{Ce}_2\text{YbCuSe}_5$, as in Figure 5. Inset shows the inverse molar magnetic susceptibility for $\text{La}_2\text{YbCuSe}_5$ at low temperature.

Table 3. Magnetic Parameters for $\text{Ln}_2\text{YbCuQ}_5$ ($\text{Ln} = \text{La}, \text{Ce}, \text{Pr}, \text{Nd}, \text{Sm}$; $\text{Q} = \text{S}, \text{Se}$)^a

formula	$P_{\text{cal}}/\mu_{\text{B}}$	100 K < T < 300 K		5 K < T < 12 K	
		$P_{\text{eff}}/\mu_{\text{B}}$	θ_{p} (K)	$P_{\text{eff}}/\mu_{\text{B}}$	θ_{p} (K)
$\text{La}_2\text{YbCuSe}_5$	4.54	4.229(9)	−38(1)	3.12(1)	−2.3(1)
$\text{Ce}_2\text{YbCuSe}_5$	5.79	5.76(1)	−54(1)	3.73(4)	−0.39(5)
$\text{La}_2\text{YbCuS}_5$	4.54	4.372(6)	−68.4(8)	2.82(2)	−2.9(2)
$\text{Ce}_2\text{YbCuS}_5$	5.79	5.31(3)	−47(2)	3.65(3)	−0.29(6)
$\text{Pr}_2\text{YbCuS}_5$	6.80	7.00(2)	−44(2)	5.44(2)	−2.2(0)
$\text{Nd}_2\text{YbCuS}_5$	6.84	6.87(1)	−46.0(8)	4.53(1)	−1.6(1)
$\text{Sm}_2\text{YbCuS}_5$	4.69	4.8(7)	−74(5)	3.06(2)	−4.9(2)

^a P_{cal} and P_{eff} : calculated and experimental effective magnetic moments per formula unit.

yet know the details of the magnetic ordering, it seems plausible that a similar situation exists here. In that case, from the temperature dependence of the susceptibility, it is more likely that only one of the ions is ferromagnetically ordered while the other ion is not ordered, down to 1.8 K. Regardless, the intriguing temperature dependence at low fields may be understood by

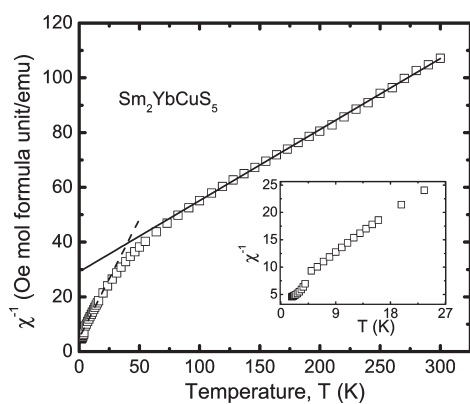


Figure 8. Inverse molar magnetic susceptibility versus temperature, showing the fit for $\text{Sm}_2\text{YbCuS}_5$, as in Figure 5. Inset shows the inverse molar magnetic susceptibility at low temperature.

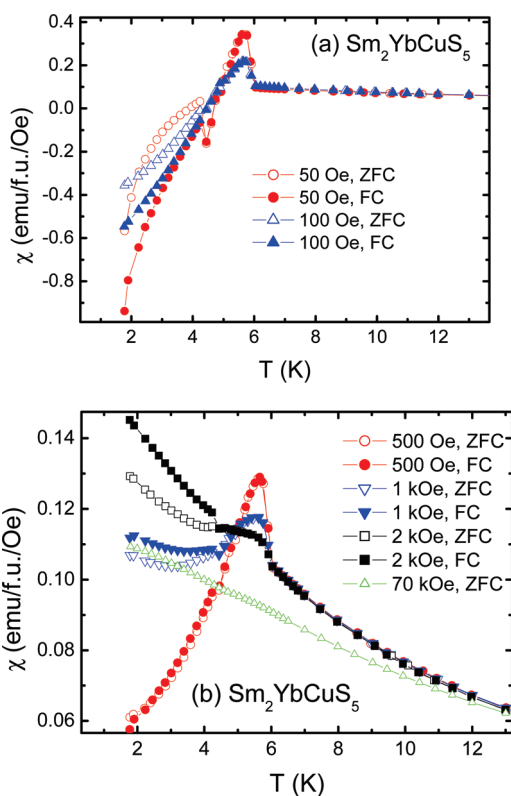


Figure 9. Magnetic susceptibility data for $\text{Sm}_2\text{YbCuS}_5$ at low temperatures under external fields of (a) 50 and 1000 Oe and (b) 0.5, 1, 2, and 70 kOe. The external field was applied and removed at 30 K. For the 70 kOe data, the difference between ZFC and FC is negligible.

antiferromagnetic coupling between the two magnetic ions: one ferromagnetically ordered at below T_c , while the moment of the other continues to increase upon cooling. Since the polarization of the latter ion increases with cooling, the temperature-induced magnetization reversal can occur below a certain temperature (T_{comp}), where the moments of the ions cancel each other, because of antiferromagnetic coupling. Because of the close proximity of T_c (5.9 K) and T_{comp} (4.5 K), the coercive field is presumably small near T_{comp} , which can explain similar behavior

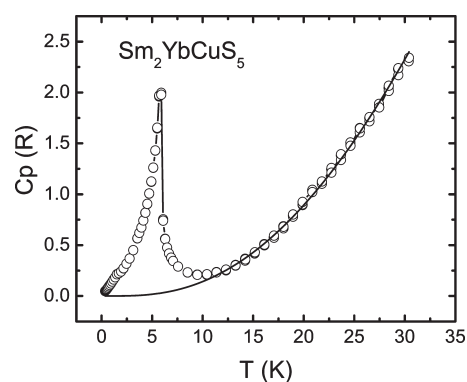


Figure 10. Temperature dependence of heat capacity of $\text{Sm}_2\text{YbCuS}_5$. The solid line is an empirical fitting curve of the lattice heat capacity (C_{ph}).

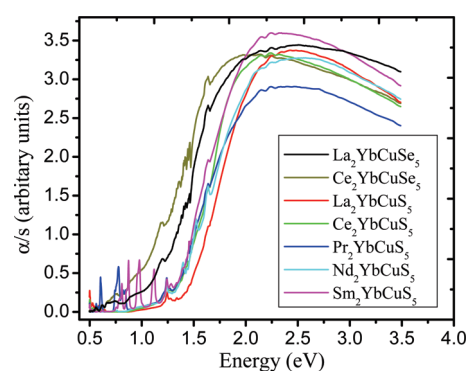


Figure 11. UV-vis diffuse reflectance spectra of $\text{Ln}_2\text{YbCuQ}_5$ ($\text{Ln} = \text{La}, \text{Ce}, \text{Pr}, \text{Nd}, \text{Sm}; \text{Q} = \text{S}, \text{Se}$).

between ZFC and FC. At higher fields, the effect of the external field weakens the antiferromagnetic coupling strength, and then the magnetization is positive.

Optical Properties. The electronic structures of interlanthanide copper chalcogenides are expected to be different from the parent interlanthanide chalcogenides after introducing more soft and electronegative Cu^+ ions into the system. Cu^+ ions prefer to bind larger chalcogenides to form more covalent bonds. This is best exhibited by the LnCuOQ series ($\text{Ln} = \text{La}, \text{Ce}, \text{Pr}, \text{Nd}; \text{Q} = \text{S}, \text{Se}, \text{Te}$),^{34–44} which consists of alternately stacked $[\text{Cu}_2\text{Q}_2]^{2-}$ layers and $[\text{Ln}_2\text{O}_2]^{2+}$ layers. The optical properties of LnCuOQ ($\text{Ln} = \text{La}, \text{Pr}, \text{Nd}; \text{Q} = \text{S}, \text{Se}, \text{Te}$) are mainly determined by $[\text{Cu}_2\text{Q}_2]^{2-}$ layers (e.g., the valence band of LaCuOTe ⁴⁴ is filled with Cu 3d and Te 5p states and the conduction band is composed of Cu 4s, Te 5p, and La 5d states; La 4f states are well above the Fermi energy). LnCuOQ ($\text{Ln} = \text{La}, \text{Pr}, \text{Nd}; \text{Q} = \text{S}, \text{Se}$) are determined to be direct allowed p -type semiconductors with wide band gaps, while the corresponding tellurides have indirect-type gaps.^{41,44} In contrast, recent studies have shown that Ce 4f states in CeCuOS and $\text{CeCu}_{0.75}\text{OS}$ compounds are fully spin-polarized and delocalized, resulting in black colors and much smaller band gaps.⁴² Another series of compounds with layered structures, LnCuS_2 ($\text{Ln} = \text{La}, \text{Nd}, \text{Sm}, \text{Gd}, \text{Dy}, \text{Ho}, \text{Yb}, \text{Lu}, \text{Y}$), are also wide-band-gap p -type semiconductors.² The substitution of larger chalcogenides narrows the band gaps by increasing the covalency in the Cu–Q bonds to lift the Fermi levels.^{33,41}

The optical properties for $\text{Ln}_2\text{YbCuQ}_5$ ($\text{Ln} = \text{La, Ce, Pr, Nd, Sm}$; $\text{Q} = \text{S, Se}$) were measured by UV–vis–NIR diffuse reflectance spectroscopy. The spectra are presented in Figure 11. The band gaps of $\text{La}_2\text{YbCuSe}_5$, $\text{Ce}_2\text{YbCuSe}_5$, $\text{La}_2\text{YbCuS}_5$, $\text{Ce}_2\text{YbCuS}_5$, $\text{Pr}_2\text{YbCuS}_5$, $\text{Nd}_2\text{YbCuS}_5$, and $\text{Sm}_2\text{YbCuS}_5$ are determined to be 1.15, 1.05, 1.45, 1.37, 1.25, 1.35, and 1.28 eV, respectively. Apparently, the selenides have smaller band gaps than the sulfides, because of the higher energy of the Se 4p orbitals. The two lanthanum compounds have somewhat larger values than the other compounds. This means that the 4f states of lanthanides other than La have some contribution to the electronic structures around the Fermi levels. $\text{Ce}_2\text{YbCuS}_5$ has slightly larger values than the Pr, Nd, and Sm cases. This behavior is unusual for many lanthanide and interlanthanide chalcogenides series, because of the high energy of the 4f¹ electron of Ce.^{62–65} Therefore, the band structures of $\text{Ln}_2\text{YbCuS}_5$ are more controlled by Cu energy levels, as expected, because of the more strongly covalent Cu–S bonds. The sharp transitions in these spectra are 4f–4f transitions for the lanthanide ions.

The band gaps of $\text{Ln}_2\text{YbCuQ}_5$ are consistent with the observed black colors, and they are reasonable, compared to SmCuS_2 (2.1 eV)⁶ and $\text{La}_3\text{CuO}_2\text{S}_3$ (2.01 eV),⁴⁶ which have less-condensed structures and lower-energy O 2p orbitals, respectively. Overall, the electronic structures of $\text{Ln}_2\text{YbCuQ}_5$ are potentially tunable, based on the choices of Ln and Q.

CONCLUSIONS

A new series of ordered quaternary interlanthanide copper chalcogenides, $\text{Ln}_2\text{YbCuQ}_5$ ($\text{Ln} = \text{La, Ce, Pr, Nd, Sm}$; $\text{Q} = \text{S, Se}$), have been synthesized using Sb_2Q_3 ($\text{Q} = \text{S, Se}$) fluxes at 900 °C. Compared to other known lanthanide copper chalcogenides, these compounds crystallize in a new structure type that is realized by including two different lanthanides with a large difference in ionic size, which tend to have distinct coordination environments. The three-dimensional complex structure of $\text{Ln}_2\text{YbCuQ}_5$ ($\text{Ln} = \text{La, Ce, Pr, Nd, Sm}$; $\text{Q} = \text{S, Se}$) includes two crystallographically unique eight-coordinated Ln atoms: one octahedral Yb site, and two Cu positions. These two Cu sites closely reside in the trigonal bipyramidal cavities formed by Q^{2-} anions that cannot be occupied simultaneously. The structure includes one-dimensional $[\text{YbCuQ}_5]^{6-}$ ribbons along the *b*-axis that are separated by larger Ln^{3+} ions. $\text{Ce}_2\text{YbCuSe}_5$, $\text{La}_2\text{YbCuS}_5$, $\text{Ce}_2\text{YbCuS}_5$, and $\text{Pr}_2\text{YbCuS}_5$ are Curie–Weiss paramagnets. $\text{La}_2\text{YbCuSe}_5$ and $\text{Nd}_2\text{YbCuS}_5$ have short-range antiferromagnetic ordering at low temperature. $\text{Sm}_2\text{YbCuS}_5$ shows evidence of long-range magnetic ordering at 5.9 K with antiferromagnetic coupling between Sm^{3+} and Yb^{3+} ions. The UV–vis–NIR diffuse reflectance measurements show these compounds to be wide-band-gap semiconductors.

ASSOCIATED CONTENT

Supporting Information. X-ray crystallographic files in CIF format for $\text{Ln}_2\text{YbCuQ}_5$ ($\text{Ln} = \text{La, Ce, Pr, Nd, Sm}$; $\text{Q} = \text{S, Se}$). This material is available free of charge via the Internet at <http://pubs.acs.org>.

AUTHOR INFORMATION

Corresponding Author

*Tel.: 574-631-1872. Fax: 574-631-9236. E-mail: talbrecl@nd.edu

ACKNOWLEDGMENT

This work was supported by the U.S. Department of Energy (DOE), under Grant DE-FG02-02ER45963 through the EPSCoR Program, and by the National Science Foundation, through No. DMR-1004459. Funds for purchasing the UV–vis–NIR spectrometer used in these studies were provided through the Chemical Sciences, Geosciences and Biosciences Division, Office of Basic Energy Sciences (OBES), Office of Science (OS), Heavy Elements Program, U.S. Department of Energy, under Grant No. DE-FG02-01ER15187. E.S.C. acknowledges support from NSF-DMR 0203532. C.H.B. acknowledges support from the Director, OS, OBES, of the U.S. DOE, under Contract No. DE-AC02-05CH11231. A portion of this work was performed at the National High Magnetic Field Laboratory, which is supported by the National Science Foundation Cooperative Agreement No. DMR-0084173, by the State of Florida, and by the Department of Energy.

REFERENCES

- (1) Julien-Pouzol, M.; Jaulmes, S.; Mazurier, A.; Guittard, M. *Acta Crystallogr., Sect. B: Struct. Crystallogr. Cryst. Chem.* **1981**, *37*, 1901.
- (2) Murugesan, T.; Gopalakrishnan, J. *Indian J. Chem.* **1983**, *22A*, 469.
- (3) Guseinov, G. G.; Amirov, A. S.; Mamedov, K. S. *Dokl. Akad. Nauk Az. SSR* **1984**, *40*, 62.
- (4) Gschneidner, K. A., Jr.; Eyring, L. R., Eds. *Handbook on the Physics and Chemistry of Rare Earths*; North-Holland Physics Publishing: New York, 1984; Vol. 6.
- (5) Wang, Y.; Sato, N.; Fujino, T. *Mater. Res. Bull.* **2001**, *36*, 1029.
- (6) Llanos, J.; Mujica, C.; Sanchez, V.; Schnelle, W.; Cardoso-Gil, R. *J. Solid State Chem.* **2004**, *177*, 1388.
- (7) Ijjaali, I.; Mitchell, K.; Ibers, J. A. *J. Solid State Chem.* **2004**, *177*, 760.
- (8) Julien-Pouzol, M.; Guittard, M.; Mazurier, A. *C. R. Acad. Sci.* **1970**, *271*, 1317.
- (9) Julien-Pouzol, M.; Guittard, M. *Ann. Chim. (Paris)* **1972**, *7*, 253.
- (10) Lauxmann, P.; Schleid, T. *Z. Anorg. Allg. Chem.* **2000**, *626*, 1608.
- (11) Dismukes, J. P.; Smith, R. T.; White, J. G. *J. Phys. Chem. Solids* **1971**, *32*, 913.
- (12) Strobel, S.; Lauxmann, P.; Schleid, T. *Z. Naturforsch.* **2005**, *60b*, 917.
- (13) Gulay, L. D.; Wolczyr, M.; Olekseyuk, I. D. *Pol. J. Chem.* **2006**, *80*, 805.
- (14) Strobel, S.; Schleid, T. *Z. Naturforsch.* **2007**, *62b*, 15.
- (15) Gulay, L. D.; Daszkiewicz, M.; Shemet, V. Ya.; Pietraszko, A. *Pol. J. Chem.* **2008**, *82*, 1001.
- (16) Daszkiewicz, M.; Gulay, L. D.; Shemet, V. Ya.; Pietraszko, A. *Z. Anorg. Allg. Chem.* **2008**, *634*, 1201.
- (17) Ballestracci, R.; Bertaut, E. F. *C. R. Acad. Sci. Paris* **1965**, *261*, 5064.
- (18) Ballestracci, R.; Bertaut, E. F. *Bull. Soc. Miner. Crystallogr.* **1965**, *88*, 575.
- (19) Guymont, M.; Thomas, A.; Julien-Pouzol, M.; Jaulmes, S.; Guittard, M. *Phys. Status Solidi A* **1990**, *121*, 21.
- (20) Onoda, M.; Chen, X. A.; Sato, A.; Wada, H. *J. Solid State Chem.* **2000**, *152*, 332.
- (21) Lemoine, P.; Carré, D.; Guittard, M. *Acta Crystallogr., Sect. C: Cryst. Struct. Commun.* **1986**, *C42*, 390.
- (22) Furuuchi, F.; Wakeshima, M.; Hinatsu, Y. *J. Solid State Chem.* **2004**, *177*, 3853.
- (23) Eu_2CuSe_3 , isostructure to Eu_2CuS_3 ; unpublished results.
- (24) Wakeshima, M.; Furuuchi, F.; Hinatsu, Y. *J. Phys.: Condens. Matter* **2004**, *16*, 5503.
- (25) Strobel, S.; Schleid, T. *Angew. Chem., Int. Ed.* **2003**, *42*, 4911.
- (26) Strobel, S.; Schleid, T. *J. Solid State Chem.* **2003**, *171*, 424.
- (27) Ijjaali, I.; Ibers, J. A. *Acta Crystallogr., Sect. E: Struct. Rep. Online* **2004**, *E39*, i89.

- (28) Gulay, L. D.; Olekseyuk, I. D. *J. Alloys Compd.* **2005**, *387*, 154.
- (29) Patschke, R.; Brazis, P.; Kannewurf, C. R.; Kanatzidis, M. G. *J. Mater. Chem.* **1999**, *9*, 2293.
- (30) Huang, F. Q.; Ibers, J. A. *J. Solid State Chem.* **2001**, *159*, 186.
- (31) Dung, N.-H.; Pardo, M.-P.; Boy, P. *Acta Crystallogr., Sect. C: Cryst. Struct. Commun.* **1983**, *C39*, 668.
- (32) Huang, F. Q.; Brazis, P.; Kannewurf, C. R.; Ibers, J. A. *J. Am. Chem. Soc.* **2000**, *122*, 80.
- (33) Huang, F. Q.; Ibers, J. A. *Inorg. Chem.* **1999**, *38*, 5978.
- (34) Popovkin, B. A.; Kusainova, A. M.; Dolgikh, V. A.; Aksel'rud, L. G. *Russ. J. Inorg. Chem.* **1998**, *43*, 1471.
- (35) Charkin, D. O.; Akopyan, A. V.; Dolgikh, V. A. *Russ. J. Inorg. Chem.* **1999**, *44*, 833.
- (36) Ueda, K.; Inoue, S.; Hirose, S.; Kawazoe, H.; Hosono, H. *Appl. Phys. Lett.* **2000**, *77*, 2701.
- (37) Ueda, K.; Inoue, S.; Hosono, H.; Sarukura, N.; Hirano, H. *Appl. Phys. Lett.* **2001**, *78*, 2333.
- (38) Inoue, S.; Ueda, K.; Hosono, H.; Hamada, N. *Phys. Rev. B* **2001**, *64*, 245211.
- (39) Ueda, K.; Takafuji, K.; Hiramatsu, H.; Ohta, H.; Kamiya, T.; Hirano, M.; Hosono, H. *Chem. Mater.* **2003**, *15*, 3692.
- (40) Ueda, K.; Takafuji, K.; Hosono, H. *J. Solid State Chem.* **2003**, *170*, 182.
- (41) Ueda, K.; Hosono, H.; Hamada, N. *J. Phys.: Condens. Matter* **2004**, *16*, 5179.
- (42) Chan, G. H.; Deng, B.; Bertoni, M.; Ireland, J. R.; Hersam, M. C.; Mason, T. O.; Van Duyne, R. P.; Ibers, J. A. *Inorg. Chem.* **2006**, *45*, 8264.
- (43) Ueda, K.; Hiramatsu, H.; Hirano, M.; Kamiya, T.; Hosono, H. *Thin Solid Films* **2006**, *496*, 8.
- (44) Liu, M. L.; Wu, L. B.; Huang, F. Q.; Chen, L. D.; Ibers, J. A. *J. Solid State Chem.* **2007**, *180*, 62.
- (45) Huang, F. Q.; Brazis, P.; Kannewurf, C. R.; Ibers, J. A. *J. Solid State Chem.* **2000**, *155*, 366.
- (46) Ijjaali, I.; Haynes, C. L.; Mcfarland, A. D.; Van Duyne, R. P.; Ibers, J. A. *J. Solid State Chem.* **2003**, *172*, 257.
- (47) Sheldrick, G. M. *SHELXTL PC, Version 6.12, An Integrated System for Solving, Refining, and Displaying Crystal Structures from Diffraction Data*; Siemens Analytical X-Ray Instruments, Inc.: Madison, WI, 2001.
- (48) Sheldrick, G. M. *SADABS 2001*, Program for absorption correction using SMART CCD based on the method of Blessing; Blessing, R. H. *Acta Crystallogr., Sect. A: Found. Crystallogr.* **1995**, *A51*, 33.
- (49) Mulay, L. N.; Boudreaux, E. A. *Theory and Applications of Molecular Diamagnetism*; Wiley-Interscience: New York, 1976.
- (50) Wendlandt, W. W.; Hecht, H. G. *Reflectance Spectroscopy*; Interscience Publishers: New York, 1966.
- (51) Shannon, R. D. *Acta Crystallogr., Sect. A: Cryst. Phys., Diffraction, Theor. Gen. Crystallogr.* **1976**, *A32*, 751.
- (52) Evans, H. T., Jr. *Nature* **1971**, *232*, 69.
- (53) Evans, H. T., Jr. *Z. Kristallogr.* **1979**, *150*, 299.
- (54) Huch, M. R.; Gulay, L. D.; Olekseyuk, I. D.; Pietraszko, A. *J. Alloys Compd.* **2006**, *425*, 230.
- (55) Huch, M. R.; Gulay, L. D.; Olekseyuk, I. D. *J. Alloys Compd.* **2007**, *439*, 156.
- (56) Gulay, L. D.; Daszkiewicz, M.; Huch, M. R.; Pietraszko, A. *Acta Crystallogr., Sect. E: Struct. Rep. Online* **2007**, *E63*, i182.
- (57) Lea, K. R.; Leask, M. J. M.; Wolf, W. A. *J. Phys. Chem. Solids* **1962**, *23*, 1381.
- (58) Ivanov, V. Y.; Mukhin, A. A.; Prokhorov, A. S.; Balbashov, A. M. *Phys. Status Solidi B* **2003**, *236*, 445.
- (59) Ohkoshi, S. I.; Iyoda, T.; Fujishima, A.; Hashimoto, K. *Phys. Rev. B* **1997**, *56*, 11642.
- (60) Egan, L.; Kamenev, K.; Papanikolaou, D.; Takabayashi, Y.; Margadonna, S. *J. Am. Chem. Soc.* **2006**, *128*, 6034.
- (61) Kovnir, K.; Thompson, C. M.; Zhou, H. D.; Wiebe, C. R.; Shatruk, M. *Chem. Mater.* **2010**, *22* (5), 1704.
- (62) Prokofiev, A. V.; Shelykh, A. I.; Golubkov, A. V.; Smirnov, I. A. *J. Alloys Compd.* **1995**, *219*, 172.
- (63) Prokofiev, A. V.; Shelykh, A. I.; Melekh, B. T. *J. Alloys Compd.* **1996**, *242*, 41.
- (64) Jin, G. B.; Choi, E. S.; Guertin, R. P.; Brooks, J. S.; Bray, T. H.; Booth, C. H.; Albrecht-Schmitt, T. E. *Chem. Mater.* **2007**, *19*, 567.
- (65) Jin, G. B.; Choi, E. S.; Guertin, R. P.; Brooks, J. S.; Bray, T. H.; Booth, C. H.; Albrecht-Schmitt, T. E. *J. Solid State Chem.* **2007**, *180*, 2129.